NANO LETTERS

Letter

pubs.acs.org/NanoLett

Role of Nonradiative Defects and Environmental Oxygen on Exciton Recombination Processes in $CsPbBr_3$ Perovskite Nanocrystals

Monica Lorenzon,[†] Luca Sortino,[†] Quinten Akkerman,[‡] Sara Accornero,[‡] Jacopo Pedrini,[†] Mirko Prato,[§] Valerio Pinchetti,[†] Francesco Meinardi,[†] Liberato Manna,*[,‡] and Sergio Brovelli*[,†]

[†]Dipartimento di Scienza dei Materiali, Università degli Studi di Milano-Bicocca, via R. Cozzi 55, 20125 Milano, Italy

[‡]Nanochemistry Department and [§]Materials Characterization Facility, Istituto Italiano di Tecnologia, via Morego 30, IT-16163 Genova, Italy

S *Supporting Information*

ABSTRACT: Lead halide perovskite nanocrystals (NCs) are emerging as optically active materials for solution-processed optoelectronic devices. Despite the technological relevance of tracing rational guidelines for optimizing their performances and stability beyond their intrinsic resilience to structural imperfections, no in-depth study of the role of selective carrier trapping and environmental conditions on their exciton dynamics has been reported to date. Here we conduct spectro-electrochemical (SEC) experiments, side-by-side to oxygen sensing measurements on $CsPbBr_3$ NCs for the first time. We show that the application of EC potentials controls the emission intensity by altering the occupancy of defect states without degrading the NCs. Reductive potentials lead to strong (60%) emission quenching by trapping of photogenerated holes, whereas the concomitant suppression of electron trapping is nearly inconsequential to the emission efficiency. Consistently, oxidizing conditions result in minor (5%) brightening due to suppressed hole trapping, confirming that electron traps play a minor role in nonradiative decay. This behavior is rationalized through a model that links the occupancy of trap sites with the position of the NC Fermi level controlled by the EC potential. Photoluminescence measurements in controlled atmosphere reveal strong quenching by collisional interactions with O_2, which is in contrast to the photobrightening effect observed in films and single crystals. This indicates that O_2 acts as a scavenger of photoexcited electrons without mediation by structural defects and, together with the asymmetrical SEC response, suggests that electron-rich defects are likely less abundant in nanostructured perovskites than in the bulk, leading to an emission response dominated by direct interaction with the environment.

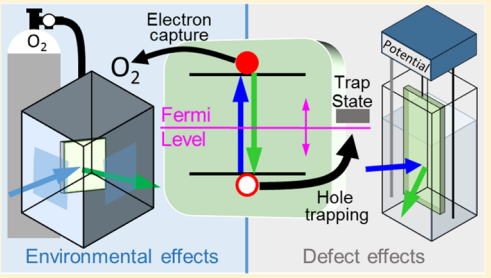

KEYWORDS: *Perovskite nanocrystals, cesium lead halide perovskites, spectro-electrochemistry, surface defects, oxygen sensing, trapping*

Lead halide perovskites are attracting growing attention as optically active materials in numerous photonics technologies,[1] including high-performance solar cells,[2−7] light-emitting diodes (LEDs),[8,9] lasers,[10−12] and radiation- and photodetectors.[13,14] Recently, colloidal synthetic routes have been developed to obtain perovskite nanocrystals (NCs) in the hybrid organic−inorganic formulation $MAPbX_3$ (MA = CH_3NH_3),[15,16] as well as in the all-inorganic cesium lead halide perovskite form, $CsPbX_3$ (X = Cl, Br, or I),[17−20] which have been demonstrated in a variety of shapes including nanocubes,[20] nanoplatelets,[18,21] nanosheets,[22] and nanowires.[16] Notably, the electronic structure and the deriving optical properties of perovskite NCs are tunable both via control of the particle size and shape (quantum confinement effect)[15,18,21] and through halide substitution via postsynthesis anion-exchange reactions,[17,20] which allow for achieving full coverage of the visible spectrum ideally suitable for wide gamut displays with ultrahigh color saturation.[11,20] For these reasons, numerous studies have recently been dedicated to the postsynthesis manipulation and assembly[23−27] of perovskite NCs, as well as to spectroscopic and device aspects including single photon emission,[28−32] exciton[33] and biexciton[34] photophysics, optical gain and lasing,[11,35−38] LEDs,[1,39−44] and solar cells.[45,46] Doping of perovskite NCs with transition metal cations such as manganese,[47−49] cadmium, zinc, tin,[50] and bismuth[51] has also been reported, resulting in widely Stokes-shifted emission from localized intragap dopant states sensitized by the NC host as well as lead-free metal−halide perovskite NCs that are technologically relevant due to toxicity concerns generated from lead-based materials.[52] A further beneficial aspect of perovskite materials is the high tolerance of their transport and photophysical properties to structural disorder, such as point defects (i.e., vacancies,[53,54] ionic rotations[55−60]), high ionic mobility[57,61] and electronic impurities,[62] which coexist with high carrier mobilities and large diffusion lengths exhibited by both films[63] and NCs.[64] This distinctive characteristic arises from their peculiar hybridized s−p antibonding valence band structure and strong spin−orbit coupling resulting in localized electronic states associated with

Received: March 24, 2017
Revised: May 3, 2017
Published: May 8, 2017

DOI: 10.1021/acs.nanolett.7b01253
Nano Lett. 2017, 17, 3844−3853

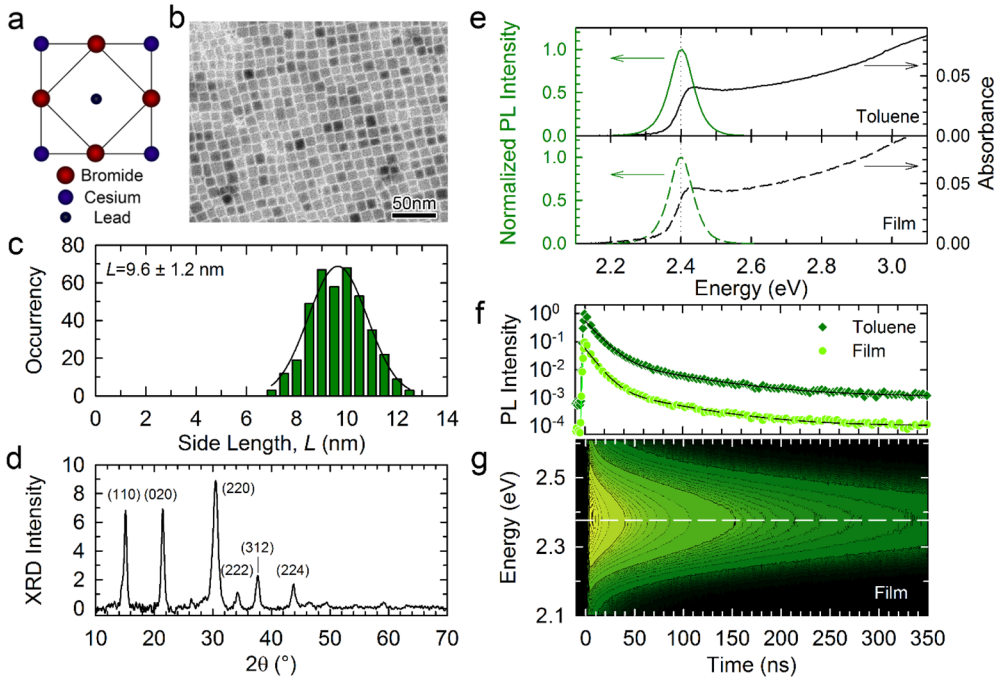

Figure 1. (a) Schematic of the crystal structure of $CsPbBr_3$ perovskites. The relative sizes are adjusted proportionally to the ionic radii of each ion (Br^-: 196 pm,[87] Cs^+: 167 pm,[87] Pb^{2+}: 120 pm[88]). (b) Transmission electron micrograph of $CsPbBr_3$ perovskite NCs and (c) related size histogram extracted from the analysis of over 300 particles, showing cubic NCs with average side length of 9.6 ± 1.2 nm. (d) X-ray diffraction pattern of $CsPbBr_3$ perovskite NCs at room temperature. (e) Optical absorption (black lines) and photoluminescence (PL, green lines) spectra of the NCs in toluene solution (top panel, solid lines) and deposited onto a silica substrate (bottom panel, dashed lines) under 3.1 eV excitation (excitation fluence 100 nJ/cm^2). (f) PL time decay curves measured at the PL maximum (2.4 eV) for the NCs in toluene (green diamonds) and in solid film (light green circles) and corresponding double-exponential fitting curve (black solid and black dashed lines for the solution and the film respectively, the curves are shifted vertically for clarity). (g) Contour plot of the PL time decay as a function of the emission energy for the NC film showing no spectral diffusion due to interdot energy transfer. The dashed white line is a guide for the eye to emphasize the invariance of the PL peak position over time.

structural defects to be positioned in energy inside the electronic bands or nearly resonant to their band edges,[65−68] rather than forming deep intragap states that in II−VI, III−V, or V−VI NCs are typically responsible for carrier trapping and nonradiative emission quenching.[69−74] As a result, both hybrid and all-inorganic perovskite NCs exhibit highly efficient narrowband photoluminescence (PL)[72,73,75−78] without the need for electronic passivation with wider-gap shells[66] commonly used to enhance the emission quantum yield of metal chalcogenides NCs and are typically less affected by photo-oxidation.[66] Nevertheless, recent studies showed that the PL and transport of both $MAPbX_3$ and $CsPbX_3$ perovskite films and single crystals are strongly affected by the environmental conditions,[79−82] leaving the role of surface defects and direct interaction with the chemical surroundings an open subject of research. Specifically, the emission efficiency was consistently observed to increase in oxygen atmosphere (both dry and humid) with respect to inert environment (vacuum or inert gases) due to passivation of photoinduced intragap states by O_2. A similar PL brightening effect has been found also in metal chalcogenide nanostructures such as CdSe nanoplatelets[72] and core/shell CdSe/CdS NCs,[73] whose emission efficiency is enhanced by molecular oxygen that, being a diradical triplet with strong electron accepting character, depletes defect states on the particle surfaces from excess electrons responsible for ultrafast nonradiative trapping of photoexcited holes in vacuum conditions.[72,73,83,84] Despite the fundamental and technological relevance of tracing rational design guidelines for optimizing the optical properties of perovskite nanostructures beyond what is already available by exploiting their intrinsic resilience to structural imperfections, no in-depth study of the role of selective carrier trapping and environmental conditions on their exciton dynamics has been reported to date.

Here, in order to investigate the nature and the effects of trap states, as well as the role of the environment in the exciton recombination process in perovskite NCs, we conduct for the first time spectro-electrochemical (SEC) experiments on $CsPbBr_3$ NCs, side-by-side to optical oxygen sensing measurements. We show that by externally tuning the position of the Fermi level through the application of an EC potential (V_{EC}), we alter the occupancy of defect states and thereby control the NC's emission intensity without degrading the NCs. Specifically, our data show that the PL efficiency is strongly quenched upon the application of a negative (reductive) V_{EC}, which corresponds to raising the Fermi level in the NC, indicating that, consistently with bulk and thin film perovskites,[79−82,85] the emission mechanism is mostly affected by trapping of photogenerated holes, whereas electron trapping plays a negligible role in nonradiative PL quenching. Accordingly, upon the application of a positive (oxidative) V_{EC}, corresponding to lowering the Fermi level in the NCs, the PL intensity increases slightly due to suppressed hole trapping in defect states depleted of excess electrons, despite the fact that oxidative conditions might concomitantly lead to the activation of electron acceptor states. The quantitative difference between the PL responses upon raising or lowering the Fermi level in the NCs, together with the relatively high PL quantum efficiency at zero EC potential (Φ_{PL} = 30 ± 4%) suggests

DOI: 10.1021/acs.nanolett.7b01253
Nano Lett. 2017, 17, 3844−3853

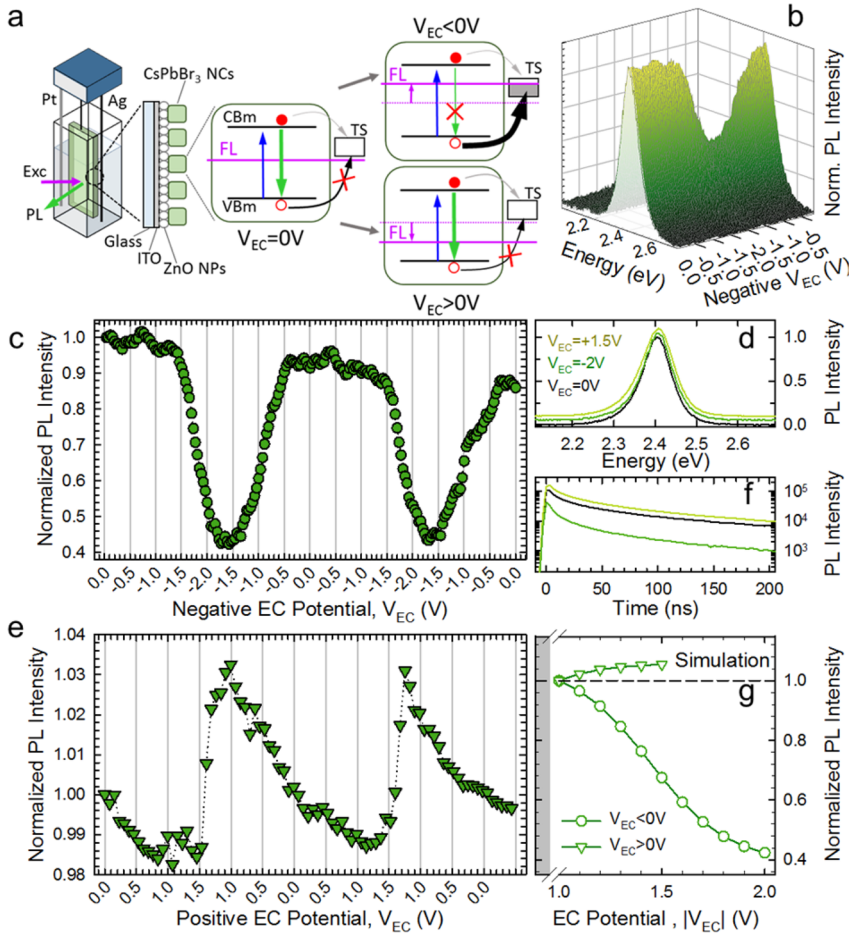

Figure 2. (a) Schematics of the SEC setup consisting of an EC cell with tetrabutylammonium perchlorate in propylene carbonate (0.1 M) as an electrolyte and a working electrode comprising an ITO-coated glass covered with a layer of ZnO nanoparticles (NPs) and $CsPbBr_3$ perovskite NCs. The figure also illustrates the radiative recombination pathway (green arrow) of photoexcited band-edge excitons and the competitive carrier trapping processes in trap states (TS). The effect of the EC potential on the PL intensity depends on the filling/emptying TS (right of the band diagram) in response to changes in the position of the Fermi level (FL; pink line). (b) A series of PL spectra (0.5 s acquisition time per frame) for a stepwise scan of the EC potential to negative values (100 mV steps each lasting 10s). (c) Spectrally integrated PL intensity as a function of V_{EC} extracted from the spectra in (b). Two sequential SEC scans are reported to show the repeatability of the measurement. (d) Normalized PL spectra at V_{EC} = 0 (black line) and V_{EC} = −2 V (green line) and VEC = +1.5 V (light green line). The spectra are shifted vertically for clarity. (e) Spectrally integrated PL intensity during a stepwise scan of the EC potential to positive values (100 mV steps each lasting 10s). Two potential scans are reported to show the repeatability of the measurement. All intensities in (c) and (e) are normalized to their values at V_{EC} = 0 V. (f) PL decay curves at V_{EC} = 0, −2, and +1.5 V. The color code is the same as in "d". All measurements are conducted using 3.1 eV excitation with fluence of 100 nJ/cm^2. (g) Simulated PL intensity versus V_{EC} for negative (circles) and positive (triangles) EC potentials. The simulation is run for V_{EC} > 1 to account for the potential step due to the ZnO interlayer.

that the number of active intragap hole traps per NC in unperturbed conditions (V_{EC} = 0 V) is arguably very small, which is in agreement with the high defect tolerance of perovskite materials.[53−61] This behavior is rationalized through a semiquantitative model that links the occupancy of trap sites to the position of the NC Fermi level. The model shows that, in the absence of EC potentials, trap sites are likely positioned in energy slightly above the Fermi level (that is, they are devoid of electrons) and their filling under negative V_{EC} leads to progressive PL quenching due to activated nonradiative hole trapping. Photoluminescence measurements in controlled oxygen atmosphere complement and extend the picture emerging from the SEC experiments and enable us to elucidate the role the NC environment on the exciton recombination dynamics. Specifically, these measurements reveal a strong effect of collisional interactions between the NCs and molecular oxygen that acts as an efficient scavenger of photogenerated electrons directly from the NC conduction band without mediation by structural defects. The removal of O_2 from the NC environment leads to nearly instantaneous and fully reversible ∼30% brightening of the PL efficiency with respect to oxygen atmosphere. This behavior indicates that the interaction mechanism between perovskite nanostructures and molecular oxygen is markedly different from the process leading to the persistent emission brightening upon O_2 exposure observed in perovskites films and single crystals,[79−81] which was ascribed to saturation of photogenerated intragap states by adsorption of O_2 molecules on the sample surface. In perovskite NCs, conversely, the PL quenching by O_2, together with the weak brightening effect of oxidative EC potentials, suggests that molecular oxygen extracts photogenerated electrons directly from the NC conduction band without the need for mediation by surface sites and further corroborates the picture that the number of electron-rich surface states acting as hole traps in

DOI: 10.1021/acs.nanolett.7b01253
Nano Lett. 2017, 17, 3844−3853

unperturbed atmospheric conditions is likely smaller than in film or bulk materials.

Results and Discussion. *Structural and Optical Properties of $CsPbBr_3$ Nanocrystals.* $CsPbBr_3$ NCs with a schematic crystal structure depicted in Figure 1a were synthesized following the procedure of Protesescu et al. (also see Methods).[17] The transmission electron microscopy image and respective size histogram reported in Figure 1b,c show particles with cubic morphology and average side length, $L = 9.6 \pm 1.2$ nm. The powder X-ray diffraction (XRD) pattern in Figure 1d confirms the orthorhombic structure of the NCs, matching with previous reports.[86]

The optical absorption and the PL spectra of the $CsPbBr_3$ NCs in toluene solution and dip-casted onto silica are reported in Figure 1e, showing identical spectral properties for the two systems with the characteristic steep absorption edge of perovskite NCs with first excitonic feature at 2.43 eV and narrow-band emission peak at 2.4 eV. The PL quantum yield is $\Phi_{PL} = 34 \pm 4\%$ in solution and $\Phi_{PL} = 30 \pm 4\%$ in solid film. Consistently, the PL decay curves collected at the emission maximum (Figure 1f) show identical decay dynamics in both solution and solid film. In agreement with previous reports,[20,28] the decay dynamics follows a double-exponential trend with a fast decay ($\tau \sim 13$ ns) responsible for ~80% of the signal followed by a longer-lived component with $\tau \sim 69$ ns accounting for the remaining ~20%. Notably, consistently with recent results by Rainò et al.,[30] the spectrally resolved contour plot of the PL decay of the NC film in Figure 1g shows no shift of the emission profile over time, indicating that spectral diffusion due to dot-to-dot energy transfer in the film is negligible, although the NCs are not coated with a wide band gap shell that has been used to suppress interdot energy transfer in close-packed films of chalcogenide NCs.[89,90]

Spectro-Electrochemistry Experiments. In order to investigate the effects of carrier trapping in intragap defects on the photophysics of $CsPbBr_3$ NCs, we conducted SEC measurements using the custom experimental setup illustrated in Figure 2a, consisting of an ITO-coated quartz substrate covered by a film of sintered ZnO particles (~50 nm diameter) and a thin layer of $CsPbBr_3$ NCs as the working electrode and silver and platinum wires as reference and counter electrodes, respectively. Figure 2a also shows a schematic band structure of the perovskite NCs with the valence band maximum (VBm) consisting of antibonding orbitals formed by s-orbitals of Pb and p-orbitals of Br and the conduction band minimum (CBm) originating from a charge transfer between p-orbitals of Pb and p-orbitals of Br, with the former providing the dominant character to the resulting orbital.[65,91,92] In unperturbed conditions, the NC Fermi level (FL) is placed at the center of the energy gap, as expected for undoped semiconductors. The intragap trap states (TS in Figure 2a) responsible for the SEC behavior are placed in energy slightly above it, according to the semiquantitative model of the EC response described later in this section.

We first apply a negative V_{EC}, which corresponds to raising the Fermi energy in the NC film, leading to progressive passivation (activation) of electron (hole) traps. In these conditions, the NC emission intensity is thus determined by the competition between the quenching effect of hole withdrawal and the brightening effect of suppressed electron trapping.

In Figure 2b, we report the complete set of PL spectra of the NCs under application of a negative V_{EC} potential scanned from 0 to −2.0 V and then back to 0 V (100 mV potential steps lasting 10 s each). To quantify the effect of the EC potential on the PL intensity, in Figure 2c we plot the integrated PL intensity as a function of V_{EC} normalized to its value at $V_{EC} = 0$ V. The measurement is repeated twice so as to assess the reversibility of the PL response and the absence of significant degradation effects. The weak ~10% PL drop, uncorrelated to the EC sweep, occurring during the whole measurement (~13 min in total) is ascribed to the dissolution of a minor population of NCs by the propylene carbonate solution. Accordingly, ~10% decrease in the optical absorbance is observed for an equivalent amount of time without the application of an EC potential (see Supporting Figure S1). In the initial stage of each potential ramp (up to $V_{EC} = -1.5$ V), no noticeable change in PL intensity occurs. This is common in SEC measurements on colloidal nanostructures using ITO/ZnO substrates[72,93−95] and is due to the combined effect of the NC coating by dielectric organic ligands and of the potential drop across the ZnO layer[96] necessary to suppress PL quenching by energy- or charge-transfer from the NCs to the ITO.[95,97] Accordingly, the current−voltage response during the SEC experiments reported in Figure S2 shows an injection threshold at ~1 V. At negative potentials above $|V_{EC}| > 1.5$ V, the PL undergoes strong quenching, reaching 60% drop of the initial emission intensity at $V_{EC} = -2$ V. When returning back to zero EC potential, for both cycles we observe almost complete recovery of the respective initial PL intensity, indicating that the potential sweeps cause no significant chemical degradation of the NCs nor permanent modifications of their surface structure. This is confirmed by the inspection of the PL spectrum collected for different V_{EC} values (Figure 2d) that shows identical emission profiles in all EC conditions. The SEC results indicate that the PL intensity trends are to be ascribed to reversible EC activation/passivation of trap sites likely associated with undercoordinated atoms or dangling bonds. Specifically, because raising the NC Fermi level under negative V_{EC} suppresses electron trapping and concomitantly activates hole traps, the observed strong drop of the PL intensity suggests that the dominant nonradiative process in our NCs is trapping of photogenerated holes, whose quenching effect on the PL efficiency is not counterbalanced by the concomitant suppression of electron trapping.

The minor role of electron trapping over hole trapping is confirmed by the SEC measurements under positive (oxidizing) EC potentials. These conditions correspond to the progressive lowering of the Fermi level in the NCs, which activates electron traps and concomitantly suppresses hole trapping by depleting surfaces states of excess electrons. Figure 2e shows the integrated PL intensity of the same NC film as Figure 2c, recorded while changing the potential from $V_{EC} = 0$ V to $V_{EC} = +1.5$ V and back to zero (0.1 V steps, 10 s per step). Also in this case, two consecutive cycles are performed to check the reproducibility of the SEC response. Same as for the negative potential ramps, for $V_{EC} < 1.5$ V, we observe no significant modification of the PL intensity except for a very weak (<1%) photobleaching. More importantly, at $V_{EC} = +1.5$ V, the trend reverses and the PL intensity increases sharply, reaching 5% enhancement with respect to its value at $V_{EC} = 0$ V. For each cycle, when sweeping the potential back to 0 V, the PL intensity returns to its initial value, indicating no permanent oxidation of the NC's surfaces. Accordingly, the PL spectrum shows no shift in energy nor the emergence of additional spectral features (Figure 2d). Therefore, similarly to the PL dimming observed under negative EC potentials, the progressive and reversible

DOI: 10.1021/acs.nanolett.7b01253
Nano Lett. 2017, 17, 3844−3853

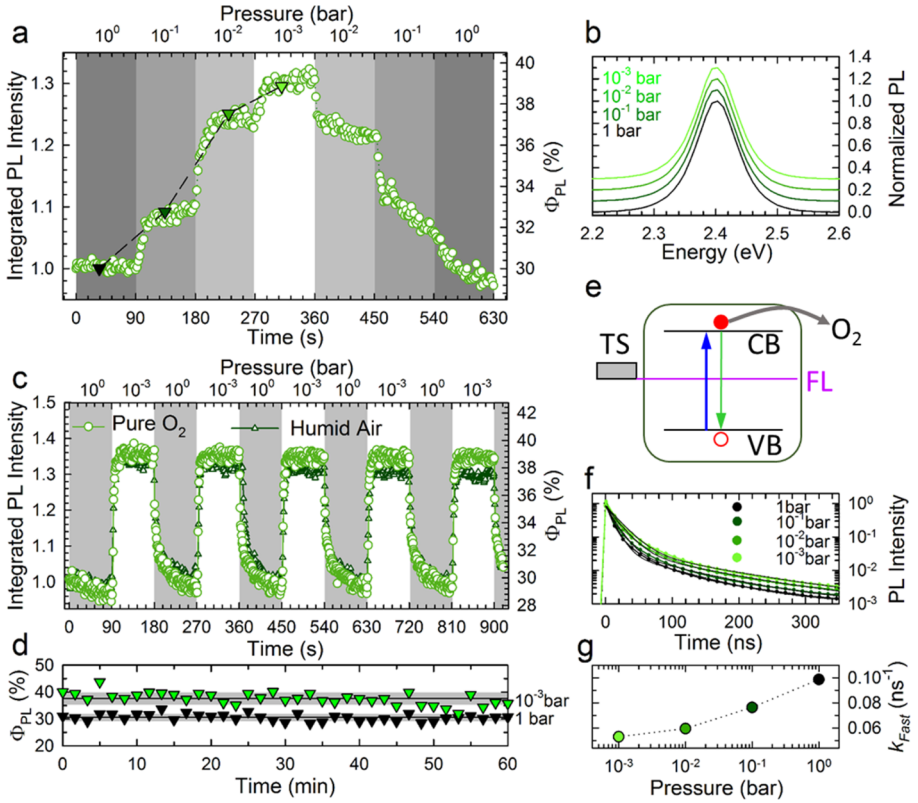

Figure 3. (a) Normalized spectrally integrated PL intensity and corresponding PL quantum yield, Φ_{PL}, of a $CsPbBr_3$ perovskite NCs film on silica during a stepwise pressure scan starting from P = 1 bar and lowering the pressure 1 order of magnitude per step, down to $P = 10^{-3}$ bar. The PL is monitored for 90 s at each pressure after which the chamber is refilled with pure O_2 following a reverse stepwise pressure ramp to P = 1 bar. (b) Normalized PL intensity at each pressure level of panel a as indicated by the symbols. The spectra are shifted vertically for clarity. (c) Normalized spectrally integrated PL intensity and corresponding PL quantum yield of $CsPbBr_3$ NCs on silica during O_2/vacuum cycles between P = 1 bar (highlighted with gray shades) and $P = 10^{-3}$ bar. (d) Φ_{PL} during continuous excitation at 3.1 eV in 10^{-3} bar vacuum (green triangles) and in 1 bar of pure O_2. (e) Schematic depiction of the interaction between O_2 and the NCs, showing direct extraction of photoexcited electrons from the conduction band (gray arrow) leading to quenching of the PL (green arrow), while surface defects (TS) placed close to the Fermi level (FL) in the absence of external potentials are essentially unaffected by oxygen. The excitation light is indicated with a blue arrow. (f) Normalized PL decay curves (dotted lines) corresponding to the pressure levels indicated by symbols in panel a and respective double-exponential fitting curves (black lines). (g) Decay rate of the fast component of the double-exponential dynamics of the NCs as a function of the O_2 pressure. All measurements are conducted using 3.1 eV excitation with fluence of 100 nJ/cm^2.

brightening under positive potential is ascribed to the EC modulation of the occupancy of surface hole traps, whose capture rate for photogenerated holes strongly outcompetes electron trapping which likely requires to overcome a larger activation energy. The same argument explains the trend for negative potentials, where filling empty defect states (inactive hole traps) with electrons markedly quenches the PL despite the fact that electron withdrawal is concomitantly reduced. Time-resolved PL traces collected for V_{EC} = 0 , −2, and +1.5 V (Figure 2f) show that the modulation of the emission intensity is due to modifications of the early time PL intensity with essentially no effect on the decay dynamics. This indicates that nonradiative hole trapping is an ultrafast process occurring prior to radiative decay, which renders a portion of NCs in the ensemble nonemissive, while the residual PL is due to the radiative decay of the subpopulation of "bright" NCs with no active hole traps. We note that the quantitative difference between the quenching and the brightening effect under negative versus positive EC potentials suggests that in the absence of an EC potential the number of active hole traps per NC is arguably small, which is in agreement with the defect tolerance of perovskite materials and the relatively high PL quantum yield of our NCs (Φ_{PL} = 30%). Accordingly, their passivation upon lowering the Fermi level in the NCs leads to markedly weaker enhancement of the emission efficiency with respect to the strong PL quenching experienced upon their activation under reductive EC potential. In both negative and positive EC potentials scans, we notice that the PL response under increasing $|V_{EC}|$ is measurably asymmetric with respect to the trend when the potential is swept back to 0 V. This effect was also observed in ZnSe and CdSe colloidal nanostructures[73,93] and is ascribed to very long lifetime of trapped carriers (up to tens of seconds)[98] with respect to the rapid capture of band edge charges in active traps resulting in the hysteresis of the PL intensity over time.

Finally, to rationalize the SEC data we propose a model that links the emission intensity (I_{PL}) to the occupancy of intragap hole traps that can be activated (passivated) by raising (lowering) the Fermi level through the application of an EC potential. The scheme of the decay channels determining the emission intensity is depicted in Figure 2a for both $V_{EC} < 0$ V and $V_{EC} > 0$ V, where trap states are positioned slightly above the Fermi level in unperturbed conditions (V_{EC} = 0 V). The application of negative potentials gradually fills TS with electrons, activating their hole trapping capability. On the other hand, lowering the FL at positive V_{EC} is nearly

DOI: 10.1021/acs.nanolett.7b01253
Nano Lett. 2017, 17, 3844−3853

inconsequential to the PL intensity, apart from the suppression of residual hole trapping. Given the negligible effect on the emission intensity observed in the SEC experiments, in the model we neglect electron trapping in order to keep the number of parameters reasonably low. To account for the effect of the EC potential on the occupancy of hole traps, we assume an average number of traps per NC, ρ_{TS}, and calculate the fraction of "bright" NCs ($F_{BRIGHT} \propto I_{PL}$) as the probability of having no active hole traps assuming a Poisson distribution across the ensemble: $F_{BRIGHT} = e^{-\mu(V_{EC})}$. Here, the term $\mu(V_{EC}) = \rho_{TS} \times \frac{1}{e^{E_{TS}-((E_F-\gamma V_{EC})/k_BT)+1}}$ is the trap density multiplied by the trap occupation probability expressed by a Fermi−Dirac distribution where E_{TS} is the energy of the trap state and $(E_F - \gamma V_{EC})$ is the Fermi energy tuned by V_{EC}. The constant γ is an attenuation factor between the applied V_{EC} and the resulting shift of the Fermi level. To illustrate the model, we calculate the EC response of our $CsPbBr_3$ NCs for a set of parameters reported in Supporting Table S1 and considering the injection potential step introduced by the ZnO interlayer that prevents electrons to reach the NCs for $V_{EC} \leq \sim 1$ V. The results of the simulations under both negative and positive V_{EC} are reported in Figure 2g. In both cases, our semiquantitative model reproduces the main experimental trends. Specifically, for $V_{EC} <$ 0 V, the progressive filling of trap states with electrons reduces the fraction of bright NCs in the ensemble, leading to 60% drop of the PL intensity. On the other hand, the PL intensity is only slightly enhanced by the application of a positive EC potential, which is in agreement with the experimental data in Figure 2e, corroborating the original scenario that in unperturbed conditions the availability of active hole traps is very small.

Oxygen Sensing Experiments. After having clarified the role of intragap defects in trapping photoexcited carriers in $CsPbBr_3$ perovskite NCs through SEC experiments, we now focus on the effect of the NC environment on the exciton recombination process. With this aim, we monitor the evolution of the PL intensity of a NC film deposited onto a glass substrate as a function of the O_2 pressure. In these experiments, the sample is kept in pure O_2 at $P = 1$ bar pressure for 90 s, after which the pressure is lowered by 1 order of magnitude at a time down to $P = 10^{-3}$ bar. For each step, the PL is monitored under constant excitation at 3.1 eV for 90 s. The ramp is then repeated while the chamber is progressively refilled with O_2 until 1 bar pressure is reestablished. The integrated PL intensity of the NC film during the pressure scan and corresponding Φ_{PL} values are reported in Figure 3a, showing a stepwise PL enhancement with decreasing O_2 pressure reaching ~30% brightening at $P = 10^{-3}$ bar with respect to atmospheric conditions with Φ_{PL} reaching ~40%.

No modification of the spectral profile is observed at any pressure level (Figure 3b), which indicates that no permanent alteration of the NCs surfaces and/or stripping of the passivating ligands occur during the pressure ramp. Accordingly, upon refilling the sample chamber with pure O_2, Φ_{PL} gradually recovers its initial value at $P = 1$ bar, indicating that the response is fully reversible and that the NCs are stable under continuous excitation for the whole duration of the measurement. The reproducibility of the PL response is further confirmed by data in Figure 3c, where we report five consecutive 90 s long ON/OFF pressure cycles between $P = 1$ bar and $P = 10^{-3}$ bar (total duration of the measurement 15 min). The same measurement is performed also using humid air (20.5 g/kg, Figure 3c) showing the same PL response than pure O_2, thus confirming that the effect is due to direct interaction with O_2 with negligible role of water vapors. The long-term stability of the NCs in O_2 and 10^{-3} bar vacuum is finally assessed by data in Figure 3d, showing constant Φ_{PL} for 1 h of continuous laser illumination at 3.1 eV. These results also corroborate our interpretation that the minor PL dimming observed in Figure 2c is a consequence of the electrolytic environment necessary for performing the SEC experiments. Notably, the PL response in Figure 3a,c follows almost instantaneously the steplike pressure change, which suggests that the increase of Φ_{PL} with decreasing O_2 pressure is due to suppression of collisional physical interactions between the NC and oxygen molecules that, owing to their strong electron affinity, extract photogenerated electrons directly from the NC conduction band. A similar effect was observed in various metal chalcogenide NCs.[72,73,99,100] A schematic depiction of the interaction mechanism is drawn in Figure 3e.

In order to gain deeper insight into the time dynamics of the NC-O_2 interaction, in Figure 3f we report the PL decay curves collected at each pressure step together with respective fit with double exponential functions. In agreement with the data in Figure 1f, for each curve we find a fast decay component accounting for over 80% of the total signal followed by a slower decay responsible for the remaining 20%. Upon lowering the O_2 pressure, the fast portion of the PL decay dynamics becomes progressively slower due to the suppression of nonradiative electron capture by O_2 molecules, while the long component remains largely unmodified. Most relevant to distinguish between so-called "static" and "dynamic" quenching mechanisms,[101] the early time PL amplitude remains constant at any investigated pressure, which suggests that PL quenching by O_2 is a dynamic process that competes with radiative exciton decay on a comparable time scale, rather than a static ultrafast mechanism, which would lower the early time PL intensity leaving the decay dynamics largely unaltered. In order to semiquantitatively describe the observed trend, in Figure 3g we report the decay rate of the fast emission that accounts for the majority of the signal ($k_{FAST} = 1/\tau_{FAST}$) at the various stages of the pressure ramp of Figure 3a. The k_{FAST}-values, obtained with no restrain of the fitting parameters, show a monotonic increase of the decay rate with increasing pressure with values scaling according to the observed difference of Φ_{PL} between the various pressure conditions (i.e., k_{FAST} ($P = 1$ bar) = 0.99 ns^{-1} is ~30% larger than the decay rate at $P = 10^{-3}$ bar (k_{FAST} ($P = 10^{-3}$ bar) = 0.074 ns^{-1}).

Finally, we point out that O_2 molecules might also adsorb onto the NC surfaces by bonding with unpaired surface electrons, leading to enhanced Φ_{PL} by suppressing their hole trapping capability, similarly to the application of a positive EC potential. This mechanism likely underpins the response to oxygen exposure of perovskite films and single crystals in refs 79−82 and determines the so-called "reverse sensing" response of bidimensional CdSe colloidal quantum wells,[72] whose Φ_{PL} is enhanced by adsorption of O_2, which passivates nonradiative hole traps that quench the PL in vacuum conditions. Therefore, similarly to the SEC trends, the overall PL brightening versus darkening response measured in oxygen sensitivity experiments provides direct insights into the competition between the two opposite effects of direct electron capture by collisional physical interactions between the NCs and O_2 molecules and their adsorption leading to passivation of unpaired surface electrons. For the perovskite NCs investigated here, the PL dimming in O_2 atmosphere indicates that direct extraction of photoexcited

DOI: 10.1021/acs.nanolett.7b01253
Nano Lett. 2017, 17, 3844−3853

conduction band electrons by collisional interaction with gaseous or physically adsorbed oxygen molecules is not counterbalanced by the passivation effect of hole traps by chemical adsorption of O_2 molecules, which is in good agreement with the weak (5%) PL brightening observed under positive EC potential (Figure 2e) and thus independently suggests that the availability of active hole traps per NC in unperturbed conditions is likely small. We highlight that the stronger impact of hole traps on the radiative decay experienced by excitons in perovskite NCs with respect to bulk or film perovskites could result from both a larger density of defects on the surfaces of the latter, as well as from the long electron−hole diffusion length[102−104] that enables photoexcited carriers to sample a large portion of the material surface and consequently be nonradiatively trapped in surface defects without their density being dramatically higher than in nanometric sized crystals.

Conclusions. In summary, we performed spectro-electrochemistry experiments and PL measurements in controlled oxygen atmosphere on $CsPbBr_3$ perovskite NCs to unveil the role of selective carrier trapping in structural defects, likely associated with surface states and dangling bonds, and the NC environment on the exciton recombination process. Results show that the main nonradiative channel in these NCs is capture of photogenerated holes in localized states that can be reversibly activated (passivated) upon raising (lowering) the Fermi level through the application of reductive (oxidizing) electrochemical potentials. As a result of the activation of hole traps, the PL is strongly quenched whereas their suppression leads to minor brightening, which strongly suggests that their density in unperturbed conditions is likely small. This feature has important consequences on the response of the NC's emission upon their exposure to oxygen gas that leads to strong quenching of the PL quantum efficiency due to the dominant effect of direct extraction of photoexcited electrons from the NC conduction band over the "curing" behavior of surface hole traps responsible for the strong PL brightening registered for perovskite films and bulk crystals. This further suggests that, despite the much larger surface to volume ratio of nanocrystals with respect to bulk or film materials, electron rich surface defects are likely less abundant in the firsts, leading to an emission response dominated by direct interaction with the environment. Our results, therefore, suggest that the interaction between perovskite NCs and atmospheric agents could be detrimental to their optical properties and thus demands specific and, possibly, more effective passivation strategies for their optimization and stabilization.

Methods. *Chemicals.* Lead(II) bromide ($PbBr_2$, 99.999% trace metals basis), cesium carbonate (Cs_2CO_3, reagentPlus, 99%), octadecene (ODE, technical grade, 90%), oleylamine (OLAM, 70%), and oleic acid (OA, 90%) were purchased from Sigma-Aldrich. Toluene (TOL, anhydrous, 99.8%) was purchased from Carlo Erba reagents. All chemicals were used without any further purification.

$CsPbBr_3$ NCs Synthesis and Purification. $CsPbBr_3$ NCs were synthesized as described by Protesescu et al.[20] with some minor adaptations. In a typical synthesis, 0.2 mmol of $PbBr_2$, 5 mL of ODE, 0.5 mL of OA and 0.5 mL of OLAM were loaded in a 25 mL 3-neck flask and dried under a vacuum for 1 h at 120 °C. After degassing, the temperature was raised to 170 °C and a mixture of 0.6 mL of ODE with 0.4 mL of previously synthesized Cs-oleate (0.4 g of Cs_2CO_3 degassed in 15 mL of ODE and 1.75 mL of OA at 150 °C) was swiftly injected. Immediately after the injection, the NC solution was quickly cooled down to room temperature with an ice bath and centrifuged for 15 min at 4000 rpm. The purified redispersed in TOL and stored in a glovebox. The films were deposited by dip-casting from a toluene solution onto glass substrates.

Spectroscopic Studies. The absorption spectra were recorded using a Varian Cary 50 spectrophotometer. The photoluminescence measurements were performed using a pulsed diode laser at 405 nm (Edinburg Inst. EPL 405, 40 ps pulse width) as excitation source and collecting the emitted light with a charged coupled device coupled to a spectrometer. Time-resolved photoluminescence experiments were conducted using the excitation source and collecting with a time-correlated single photon counting unit coupled to a monochromator and a photomultiplier tube. All PL measurements were performed with power density of 100 nJ/cm^2. All measurements were carried out at room temperature.

For oxygen pressure studies, a few monolayer films of $CsPbBr_3$ NCs were deposited on quartz substrates by dip-casting from diluted toluene solutions (optical density of 0.07 at 500 nm; 2 dips for 10 s). The films were successively mounted in a sealed chamber with direct optical access and the PL was monitored using the setup described above both as a function of the oxygen pressure and during O_2/vacuum cycles to test the reversibility of the quenching process. Before any pressure ramp, the PL efficiency has been preliminary monitored for several minutes in pure O_2 in order to evaluate possible intensity fluctuations due to UV exposure. No photobrightening has been observed for any of the investigated samples. The same procedure has been followed for PL measurements in humid air (20.5 g/kg).

Spectro-electrochemical Measurements. Indium tin oxide (ITO) coated glass slides (50 × 7 × 0.7 mm, R_S < 100Ω) were purchased from Delta Technologies (Part No. CG-90IN-CUV). The ITO coated surface was first covered with zinc oxide (ZnO) nanoparticles (NP) (Nanograde, ∼50 nm diameter) to avoid quenching of NC emission by fast charge/energy-transfer to ITO.[95,97] The ZnO NP layer (∼60 nm thick, as measured using a Dektak profilometer) was deposited by dip-coating the glass/ITO substrate into an ethanol suspension of ZnO NPs (2 mg/mL, one dip for 10 s) and annealed at 150 °C for 10 min in a nitrogen glovebox.

To test the stability of the glass/ITO/ZnO NP substrates during the potential scans, we performed control experiments in which we monitored changes in optical absorption spectra for prolonged exposures to negative and positive potentials.[105] The results of these measurements indicate that the substrates are unaffected by either positive or negative electrochemical potentials for exposure times of tens of minutes, which are much longer than the measurement time used in our SEC experiments (∼10 min).

The NCs were deposited onto the ZnO NP layer as a few-monolayer-thick film by dip-coating from a dilute toluene solution (optical density of 0.07 at 500 nm; 2 dips for 10 s). The ZnO NPs layer used in this study was not treated with cross-linkers as in ref 95 and therefore it represented a dielectric tunneling barrier between the ITO electrode and the NC film. As a result of a voltage drop across the ZnO NP layer, the NCs experienced a reduced potential; according to our estimations, the attenuation factor was approximately 0.13 and the activation of the EC response requires to overcome an injection barrier of ∼1 V. The ITO was connected as a working electrode to the potentiostat (Bio Logic SP-200 Research grade

DOI: 10.1021/acs.nanolett.7b01253
Nano Lett. 2017, 17, 3844−3853

Potentiostat/Galvanostat) and the film was placed into a quartz cuvette filled with the electrolyte (0.1 M tetrabutylammonium perchlorate ($TBAClO_4$) in propylene carbonate). Silver and platinum wires were used as quasi-reference and counter electrodes, respectively. All potentials reported in this work are measured relative to the quasi-reference silver electrode during staircase voltammetry scans (10 s scan rate).

The film was excited at 3.1 eV with continuous wave diode lasers and the emitted light was collected with a focusing lens and sent to a spectrometer coupled to a charge coupled device (CCD) array for spectral measurements.

■ ASSOCIATED CONTENT

Supporting Information

The Supporting Information is available free of charge on the ACS Publications website at DOI: 10.1021/acs.nanolett.7b01253.

Figure S1: Absorption spectra of $CsPbBr_3$NCs film immersed in propylene carbonate collected every 300 s over a 30 min time interval. Figure S2: Current−voltage response collected during a spectro-electrochemical scan. Table S1: Parameters used to reproduce the spectro-electrochemical trends. (PDF)

■ AUTHOR INFORMATION

Corresponding Authors

*E-mail: sergio.brovelli@unimib.it. Telephone: +39 02 6448 5027.

*E-mail: liberato.manna@iit.it. Telephone: +39 010 71781 502.

ORCID

Monica Lorenzon: 0000-0003-3524-9546

Mirko Prato: 0000-0002-2188-8059

Valerio Pinchetti: 0000-0003-3792-3661

Liberato Manna: 0000-0003-4386-7985

Sergio Brovelli: 0000-0002-5993-855X

Author Contributions

The manuscript was written through contributions of all authors. All authors have given approval to the final version of the manuscript.

Notes

The authors declare no competing financial interest.

■ ACKNOWLEDGMENTS

S.B. wishes to thank the European Community's Seventh Framework Programme (FP7/2007-2013) under Grant Agreement 324603 for financial support (EDONHIST) and Cariplo Foundation (2012-0844, 2012-0920). M.L. thanks the Fondazione Cassa di Risparmio di Tortona for support. L.M acknowledges funding from the seventh European Community Framework Programme under Grant Agreement 614897 (ERC Consolidator Grant "TRANS-NANO") and from Framework Programme for Research and Innovation Horizon 2020 (2014-2020) under the Marie Skłodowska-Curie Grant Agreement COMPASS No. 691185.

■ REFERENCES

(1) Sutherland, B. R.; Sargent, E. H. *Nat. Photonics* **2016**, *10*, 295−302.

(2) Green, M. A.; Ho-Baillie, A.; Snaith, H. J. *Nat. Photonics* **2014**, *8*, 506−514.

(3) Park, N.-G. *J. Phys. Chem. Lett.* **2013**, *4*, 2423−2429.

(4) Service, R. F. *Science* **2014**, *344*, 458−458.

(5) Snaith, H. J. *J. Phys. Chem. Lett.* **2013**, *4*, 3623−3630.

(6) Tsai, H.; Nie, W.; Blancon, J.-C.; Stoumpos, C. C.; Asadpour, R.; Harutyunyan, B.; Neukirch, A. J.; Verduzco, R.; Crochet, J. J.; Tretiak, S.; Pedesseau, L.; Even, J.; Alam, M. A.; Gupta, G.; Lou, J.; Ajayan, P. M.; Bedzyk, M. J.; Kanatzidis, M. G.; Mohite, A. D. *Nature* **2016**, *536*, 312−316.

(7) Nie, W.; Tsai, H.; Asadpour, R.; Blancon, J.-C.; Neukirch, A. J.; Gupta, G.; Crochet, J. J.; Chhowalla, M.; Tretiak, S.; Alam, M. A.; Wang, H.-L.; Mohite, A. D. *Science* **2015**, *347*, 522−525.

(8) Tan, Z.-K.; Moghaddam, R. S.; Lai, M. L.; Docampo, P.; Higler, R.; Deschler, F.; Price, M.; Sadhanala, A.; Pazos, L. M.; Credgington, D.; Hanusch, F.; Bein, T.; Snaith, H. J.; Friend, R. H. *Nat. Nanotechnol.* **2014**, *9*, 687−692.

(9) Zhang, F.; Zhong, H.; Chen, C.; Wu, X.-g.; Hu, X.; Huang, H.; Han, J.; Zou, B.; Dong, Y. *ACS Nano* **2015**, *9*, 4533−4542.

(10) Xing, G.; Mathews, N.; Lim, S. S.; Yantara, N.; Liu, X.; Sabba, D.; Grätzel, M.; Mhaisalkar, S.; Sum, T. C. *Nat. Mater.* **2014**, *13*, 476−480.

(11) Yakunin, S.; Protesescu, L.; Krieg, F.; Bodnarchuk, M. I.; Nedelcu, G.; Humer, M.; De Luca, G.; Fiebig, M.; Heiss, W.; Kovalenko, M. V. *Nat. Commun.* **2015**, *6*, 8056.

(12) Zhu, H.; Fu, Y.; Meng, F.; Wu, X.; Gong, Z.; Ding, Q.; Gustafsson, M. V.; Trinh, M. T.; Jin, S.; Zhu, X. Y. *Nat. Mater.* **2015**, *14*, 636−642.

(13) Chen, S.; Shi, G. *Adv. Mater.* **2017**, 1605448.

(14) Yakunin, S.; Sytnyk, M.; Kriegner, D.; Shrestha, S.; Richter, M.; Matt, G. J.; Azimi, H.; Brabec, C. J.; Stangl, J.; Kovalenko, M. V.; Heiss, W. *Nat. Photonics* **2015**, *9*, 444−449.

(15) Sichert, J. A.; Tong, Y.; Mutz, N.; Vollmer, M.; Fischer, S.; Milowska, K. Z.; García Cortadella, R.; Nickel, B.; Cardenas-Daw, C.; Stolarczyk, J. K.; Urban, A. S.; Feldmann, J. *Nano Lett.* **2015**, *15*, 6521−6527.

(16) Zhang, D.; Eaton, S. W.; Yu, Y.; Dou, L.; Yang, P. *J. Am. Chem. Soc.* **2015**, *137*, 9230−9233.

(17) Akkerman, Q. A.; D'Innocenzo, V.; Accornero, S.; Scarpellini, A.; Petrozza, A.; Prato, M.; Manna, L. *J. Am. Chem. Soc.* **2015**, *137*, 10276−10281.

(18) Akkerman, Q. A.; Motti, S. G.; Srimath Kandada, A. R.; Mosconi, E.; D'Innocenzo, V.; Bertoni, G.; Marras, S.; Kamino, B. A.; Miranda, L.; De Angelis, F.; Petrozza, A.; Prato, M.; Manna, L. *J. Am. Chem. Soc.* **2016**, *138*, 1010−1016.

(19) Nedelcu, G.; Protesescu, L.; Yakunin, S.; Bodnarchuk, M. I.; Grotevent, M. J.; Kovalenko, M. V. *Nano Lett.* **2015**, *15*, 5635−5640.

(20) Protesescu, L.; Yakunin, S.; Bodnarchuk, M. I.; Krieg, F.; Caputo, R.; Hendon, C. H.; Yang, R. X.; Walsh, A.; Kovalenko, M. V. *Nano Lett.* **2015**, *15*, 3692−3696.

(21) Bekenstein, Y.; Koscher, B. A.; Eaton, S. W.; Yang, P.; Alivisatos, A. P. *J. Am. Chem. Soc.* **2015**, *137*, 16008−16011.

(22) Shamsi, J.; Dang, Z.; Bianchini, P.; Canale, C.; Stasio, F. D.; Brescia, R.; Prato, M.; Manna, L. *J. Am. Chem. Soc.* **2016**, *138*, 7240−7243.

(23) Kim, Y.; Yassitepe, E.; Voznyy, O.; Comin, R.; Walters, G.; Gong, X.; Kanjanaboos, P.; Nogueira, A. F.; Sargent, E. H. *ACS Appl. Mater. Interfaces* **2015**, *7*, 25007−25013.

(24) Palazon, F.; Akkerman, Q. A.; Prato, M.; Manna, L. *ACS Nano* **2016**, *10*, 1224−1230.

(25) De Roo, J.; Ibáñez, M.; Geiregat, P.; Nedelcu, G.; Walravens, W.; Maes, J.; Martins, J. C.; Van Driessche, I.; Kovalenko, M. V.; Hens, Z. *ACS Nano* **2016**, *10*, 2071−2081.

(26) Huang, H.; Chen, B.; Wang, Z.; Hung, T. F.; Susha, A. S.; Zhong, H.; Rogach, A. L. *Chem. Sci.* **2016**, *7*, 5699−5703.

(27) Zhang, X.; Lv, L.; Ji, L.; Guo, G.; Liu, L.; Han, D.; Wang, B.; Tu, Y.; Hu, J.; Yang, D.; Dong, A. *J. Am. Chem. Soc.* **2016**, *138*, 3290−3293.

(28) Makarov, N. S.; Guo, S.; Isaienko, O.; Liu, W.; Robel, I.; Klimov, V. I. *Nano Lett.* **2016**, *16*, 2349−2362.

(29) Park, Y.-S.; Guo, S.; Makarov, N. S.; Klimov, V. I. *ACS Nano* **2015**, *9*, 10386−10393.

DOI: 10.1021/acs.nanolett.7b01253
Nano Lett. 2017, 17, 3844−3853

(30) Rainò, G.; Nedelcu, G.; Protesescu, L.; Bodnarchuk, M. I.; Kovalenko, M. V.; Mahrt, R. F.; Stöferle, T. *ACS Nano* **2016**, *10*, 2485−2490.
(31) Swarnkar, A.; Chulliyil, R.; Ravi, V. K.; Irfanullah, M.; Chowdhury, A.; Nag, A. *Angew. Chem., Int. Ed.* **2015**, *54*, 15424−15428.
(32) Tian, Y.; Merdasa, A.; Peter, M.; Abdellah, M.; Zheng, K.; Ponseca, C. S.; Pullerits, T.; Yartsev, A.; Sundström, V.; Scheblykin, I. G. *Nano Lett.* **2015**, *15*, 1603−1608.
(33) Fu, M.; Tamarat, P.; Huang, H.; Even, J.; Rogach, A. L.; Lounis, B. *Nano Lett.* **2017**.
(34) Castañeda, J. A.; Nagamine, G.; Yassitepe, E.; Bonato, L. G.; Voznyy, O.; Hoogland, S.; Nogueira, A. F.; Sargent, E. H.; Cruz, C. H. B.; Padilha, L. A. *ACS Nano* **2016**, *10*, 8603−8609.
(35) Eaton, S. W.; Lai, M.; Gibson, N. A.; Wong, A. B.; Dou, L.; Ma, J.; Wang, L.-W.; Leone, S. R.; Yang, P. *Proc. Natl. Acad. Sci. U. S. A.* **2016**, *113*, 1993−1998.
(36) Wang, Y.; Li, X.; Song, J.; Xiao, L.; Zeng, H.; Sun, H. *Adv. Mater.* **2015**, *27*, 7101−7108.
(37) Wang, Y.; Li, X.; Zhao, X.; Xiao, L.; Zeng, H.; Sun, H. *Nano Lett.* **2016**, *16*, 448−453.
(38) Xu, Y.; Chen, Q.; Zhang, C.; Wang, R.; Wu, H.; Zhang, X.; Xing, G.; Yu, W. W.; Wang, X.; Zhang, Y.; Xiao, M. *J. Am. Chem. Soc.* **2016**, *138*, 3761−3768.
(39) Yassitepe, E.; Yang, Z.; Voznyy, O.; Kim, Y.; Walters, G.; Castañeda, J. A.; Kanjanaboos, P.; Yuan, M.; Gong, X.; Fan, F.; Pan, J.; Hoogland, S.; Comin, R.; Bakr, O. M.; Padilha, L. A.; Nogueira, A. F.; Sargent, E. H. *Adv. Funct. Mater.* **2016**, *26*, 8757−8763.
(40) Li, G.; Rivarola, F. W. R.; Davis, N. J. L. K.; Bai, S.; Jellicoe, T. C.; de la Peña, F.; Hou, S.; Ducati, C.; Gao, F.; Friend, R. H.; Greenham, N. C.; Tan, Z.-K. *Adv. Mater.* **2016**, *28*, 3528−3534.
(41) Palazon, F.; Di Stasio, F.; Akkerman, Q. A.; Krahne, R.; Prato, M.; Manna, L. *Chem. Mater.* **2016**, *28*, 2902−2906.
(42) Song, J.; Li, J.; Li, X.; Xu, L.; Dong, Y.; Zeng, H. *Adv. Mater.* **2015**, *27*, 7162−7167.
(43) Zhang, X.; Lin, H.; Huang, H.; Reckmeier, C.; Zhang, Y.; Choy, W. C. H.; Rogach, A. L. *Nano Lett.* **2016**, *16*, 1415−1420.
(44) Zhang, X.; Xu, B.; Zhang, J.; Gao, Y.; Zheng, Y.; Wang, K.; Sun, X. W. *Adv. Funct. Mater.* **2016**, *26*, 4595−4600.
(45) Swarnkar, A.; Marshall, A. R.; Sanehira, E. M.; Chernomordik, B. D.; Moore, D. T.; Christians, J. A.; Chakrabarti, T.; Luther, J. M. *Science* **2016**, *354*, 92−95.
(46) Akkerman, Q. A.; Gandini, M.; Di Stasio, F.; Rastogi, P.; Palazon, F.; Bertoni, G.; Ball, J. M.; Prato, M.; Petrozza, A.; Manna, L. *Nat. Energy* **2016**, *2*, 16194.
(47) Liu, W.; Lin, Q.; Li, H.; Wu, K.; Robel, I.; Pietryga, J. M.; Klimov, V. I. *J. Am. Chem. Soc.* **2016**.
(48) Parobek, D.; Roman, B. J.; Dong, Y.; Jin, H.; Lee, E.; Sheldon, M.; Son, D. H. *Nano Lett.* **2016**, *16*, 7376−7380.
(49) Mir, W. J.; Jagadeeswararao, M.; Das, S.; Nag, A. *ACS Energy Lett.* **2017**, *2*, 537−543.
(50) van der Stam, W.; Geuchies, J. J.; Altantzis, T.; van den Bos, K. H. W.; Meeldijk, J. D.; Van Aert, S.; Bals, S.; Vanmaekelbergh, D.; de Mello Donega, C. *J. Am. Chem. Soc.* **2017**, *139*, 4087−4097.
(51) Begum, R.; Parida, M. R.; Abdelhady, A. L.; Murali, B.; Alyami, N. M.; Ahmed, G. H.; Hedhili, M. N.; Bakr, O. M.; Mohammed, O. F. *J. Am. Chem. Soc.* **2017**, *139*, 731−737.
(52) Swarnkar, A.; Ravi, V. K.; Nag, A. *ACS Energy Lett.* **2017**, 1089−1098.
(53) Frost, J. M.; Butler, K. T.; Brivio, F.; Hendon, C. H.; van Schilfgaarde, M.; Walsh, A. *Nano Lett.* **2014**, *14*, 2584−2590.
(54) Walsh, A.; Scanlon, D. O.; Chen, S.; Gong, X. G.; Wei, S.-H. *Angew. Chem.* **2015**, *127*, 1811−1814.
(55) Bakulin, A. A.; Selig, O.; Bakker, H. J.; Rezus, Y. L. A.; Müller, C.; Glaser, T.; Lovrincic, R.; Sun, Z.; Chen, Z.; Walsh, A.; Frost, J. M.; Jansen, T. L. C. *J. Phys. Chem. Lett.* **2015**, *6*, 3663−3669.
(56) Brivio, F.; Walker, A. B.; Walsh, A. *APL Mater.* **2013**, *1*, 042111.
(57) Leguy, A. M. A.; Frost, J. M.; McMahon, A. P.; Sakai, V. G.; Kockelmann, W.; Law, C.; Li, X.; Foglia, F.; Walsh, A.; O'Regan, B. C.; Nelson, J.; Cabral, J. T.; Barnes, P. R. F. *Nat. Commun.* **2015**, *6*, 7124.
(58) Quarti, C.; Mosconi, E.; De Angelis, F. *Phys. Chem. Chem. Phys.* **2015**, *17*, 9394−9409.
(59) Quarti, C.; Mosconi, E.; De Angelis, F. *Chem. Mater.* **2014**, *26*, 6557−6569.
(60) Brivio, F.; Frost, J. M.; Skelton, J. M.; Jackson, A. J.; Weber, O. J.; Weller, M. T.; Goñi, A. R.; Leguy, A. M. A.; Barnes, P. R. F.; Walsh, A. *Phys. Rev. B: Condens. Matter Mater. Phys.* **2015**, *92*, 144308.
(61) Mosconi, E.; De Angelis, F. *ACS Energy Lett.* **2016**, *1*, 182−188.
(62) Blancon, J.-C.; Nie, W.; Neukirch, A. J.; Gupta, G.; Tretiak, S.; Cognet, L.; Mohite, A. D.; Crochet, J. J. *Adv. Funct. Mater.* **2016**, *26*, 4283−4292.
(63) Wehrenfennig, C.; Eperon, G. E.; Johnston, M. B.; Snaith, H. J.; Herz, L. M. *Adv. Mater.* **2014**, *26*, 1584−1589.
(64) Yettapu, G. R.; Talukdar, D.; Sarkar, S.; Swarnkar, A.; Nag, A.; Ghosh, P.; Mandal, P. *Nano Lett.* **2016**, *16*, 4838−4848.
(65) Brandt, R. E.; Stevanović, V.; Ginley, D. S.; Buonassisi, T. *MRS Commun.* **2015**, *5*, 265−275.
(66) Dirin, D. N.; Protesescu, L.; Trummer, D.; Kochetygov, I. V.; Yakunin, S.; Krumeich, F.; Stadie, N. P.; Kovalenko, M. V. *Nano Lett.* **2016**, *16*, 5866−5874.
(67) Kang, J.; Wang, L.-W. *J. Phys. Chem. Lett.* **2017**, *8*, 489−493.
(68) Zakutayev, A.; Caskey, C. M.; Fioretti, A. N.; Ginley, D. S.; Vidal, J.; Stevanovic, V.; Tea, E.; Lany, S. *J. Phys. Chem. Lett.* **2014**, *5*, 1117−1125.
(69) Qin, H.; Meng, R.; Wang, N.; Peng, X. *Adv. Mater.* **2017**, *29*, 1606923.
(70) Choi, J.-H.; Oh, S. J.; Lai, Y.; Kim, D. K.; Zhao, T.; Fafarman, A. T.; Diroll, B. T.; Murray, C. B.; Kagan, C. R. *ACS Nano* **2013**, *7*, 8275−8283.
(71) Feng, Y.; Cheng, J.; Zhou, L.; Zhou, X.; Xiang, H. *Analyst* **2012**, *137*, 4885−4901.
(72) Lorenzon, M.; Christodoulou, S.; Vaccaro, G.; Pedrini, J.; Meinardi, F.; Moreels, I.; Brovelli, S. *Nat. Commun.* **2015**, *6*, 6434.
(73) Lorenzon, M.; Pinchetti, V.; Bruni, F.; Bae, W. K.; Meinardi, F.; Klimov, V. I.; Brovelli, S. *Nano Lett.* **2017**, *17*, 1071−1081.
(74) Saba, M.; Aresti, M.; Quochi, F.; Marceddu, M.; Loi, M. A.; Huang, J.; Talapin, D. V.; Mura, A.; Bongiovanni, G. *ACS Nano* **2013**, *7*, 229−238.
(75) Abate, A.; Saliba, M.; Hollman, D. J.; Stranks, S. D.; Wojciechowski, K.; Avolio, R.; Grancini, G.; Petrozza, A.; Snaith, H. J. *Nano Lett.* **2014**, *14*, 3247−3254.
(76) Han, P.; Mihi, A.; Ferre-borrull, J.; Pallarés, J.; Marsal, L. F. *J. Phys. Chem. C* **2015**, *119*, 10693−10699.
(77) Hens, Z.; Moreels, I.; Martins, J. C. *ChemPhysChem* **2005**, *6*, 2578−2584.
(78) Xu, S.; Ziegler, J.; Nann, T. *J. Mater. Chem.* **2008**, *18*, 2653−2656.
(79) Motti, S. G.; Gandini, M.; Barker, A. J.; Ball, J. M.; Srimath Kandada, A. R.; Petrozza, A. *ACS Energy Lett.* **2016**, *1*, 726−730.
(80) Galisteo-López, J. F.; Anaya, M.; Calvo, M. E.; Míguez, H. *J. Phys. Chem. Lett.* **2015**, *6*, 2200−2205.
(81) Fang, H.-H.; Adjokatse, S.; Wei, H.; Yang, J.; Blake, G. R.; Huang, J.; Even, J.; Loi, M. A. *Sci. Adv.* **2016**, *2*, e1600534.
(82) Tian, Y.; Merdasa, A.; Unger, E.; Abdellah, M.; Zheng, K.; McKibbin, S.; Mikkelsen, A.; Pullerits, T.; Yartsev, A.; Sundström, V.; Scheblykin, I. G. *J. Phys. Chem. Lett.* **2015**, *6*, 4171−4177.
(83) Javaux, C.; Mahler, B.; Dubertret, B.; Shabaev, A.; Rodina, A. V.; EfrosAl, L.; Yakovlev, D. R.; Liu, F.; Bayer, M.; Camps, G.; Biadala, L.; Buil, S.; Quelin, X.; Hermier, J. P. *Nat. Nanotechnol.* **2013**, *8*, 206−212.
(84) Liu, F.; Biadala, L.; Rodina, A. V.; Yakovlev, D. R.; Dunker, D.; Javaux, C.; Hermier, J.-P.; Efros, A. L.; Dubertret, B.; Bayer, M. *Phys. Rev. B: Condens. Matter Mater. Phys.* **2013**, *88*, 035302.
(85) Leijtens, T.; Eperon, G. E.; Barker, A. J.; Grancini, G.; Zhang, W.; Ball, J. M.; Kandada, A. R. S.; Snaith, H. J.; Petrozza, A. *Energy Environ. Sci.* **2016**, *9*, 3472−3481.

DOI: 10.1021/acs.nanolett.7b01253
Nano Lett. 2017, 17, 3844−3853

(86) Cottingham, P.; Brutchey, R. L. *Chem. Commun.* **2016**, *52*, 5246−5249.
(87) Slater, J. C. *J. Chem. Phys.* **1964**, *41*, 3199−3204.
(88) Ahrens, L. H. *Geochim. Cosmochim. Acta* **1952**, *2*, 155−169.
(89) Crooker, S. A.; Barrick, T.; Hollingsworth, J. A.; Klimov, V. I. *Appl. Phys. Lett.* **2003**, *82*, 2793−2795.
(90) Pal, B. N.; Ghosh, Y.; Brovelli, S.; Laocharoensuk, R.; Klimov, V. I.; Hollingsworth, J. A.; Htoon, H. *Nano Lett.* **2012**, *12*, 331−336.
(91) Niimi, T.; Yoshida, M.; Kondo, M.; Oshima, Y.; Mori, H.; Egami, Y.; Asai, K.; Nishide, H. *J. Thermophys. Heat Transfer* **2005**, *19*, 9−16.
(92) Ravi, V. K.; Markad, G. B.; Nag, A. *ACS Energy Lett.* **2016**, *1*, 665−671.
(93) Brovelli, S.; Galland, C.; Viswanatha, R.; Klimov, V. I. *Nano Lett.* **2012**, *12*, 4372−4379.
(94) Galland, C.; Ghosh, Y.; Steinbrueck, A.; Sykora, M.; Hollingsworth, J. A.; Klimov, V. I.; Htoon, H. *Nature* **2011**, *479*, 203−207.
(95) Jha, P. P.; Guyot-Sionnest, P. *J. Phys. Chem. C* **2010**, *114*, 21138−21141.
(96) Dewald, J. F. *J. Phys. Chem. Solids* **1960**, *14*, 155−161.
(97) Jin, S.; Song, N.; Lian, T. *ACS Nano* **2010**, *4*, 1545−1552.
(98) Padilha, L. A.; Robel, I.; Lee, D. C.; Nagpal, P.; Pietryga, J. M.; Klimov, V. I. *ACS Nano* **2011**, *5*, 5045−5055.
(99) Müller, J.; Lupton, J. M.; Rogach, A. L.; Feldmann, J.; Talapin, D. V.; Weller, H. *Appl. Phys. Lett.* **2004**, *85*, 381−383.
(100) Nazzal, A. Y.; Qu, L.; Peng, X.; Xiao, M. *Nano Lett.* **2003**, *3*, 819−822.
(101) Lakowicz, J. *Principles of Fluorescence Spectroscopy*. 3rd ed.; Springer:, 2006.
(102) Stranks, S. D.; Eperon, G. E.; Grancini, G.; Menelaou, C.; Alcocer, M. J. P.; Leijtens, T.; Herz, L. M.; Petrozza, A.; Snaith, H. J. *Science* **2013**, *342*, 341−344.
(103) Li, Y.; Yan, W.; Li, Y.; Wang, S.; Wang, W.; Bian, Z.; Xiao, L.; Gong, Q. *Sci. Rep.* **2015**, *5*, 14485.
(104) Xing, G.; Mathews, N.; Sun, S.; Lim, S. S.; Lam, Y. M.; Grätzel, M.; Mhaisalkar, S.; Sum, T. C. *Science* **2013**, *342*, 344−347.
(105) Senthilkumar, M.; Mathiyarasu, J.; Joseph, J.; Phani, K. L. N.; Yegnaraman, V. *Mater. Chem. Phys.* **2008**, *108*, 403−407.

DOI: 10.1021/acs.nanolett.7b01253
Nano Lett. 2017, 17, 3844−3853